Robustness of Vegetation Optical Depth Retrievals Based on L-Band Global Radiometry

David Chaparro, Andrew F. Feldman, *Member, IEEE,* Mario J. Chaubell, Simon H. Yueh, *Fellow, IEEE,* Dara Entekhabi, *Fellow, IEEE*

***Abstract*— Microwave vegetation optical depth (VOD) and soil moisture (SM) can be simultaneously retrieved based on L-band radiometry with polarization information. VOD is indicative of the vegetation water content (VWC) because it captures the extinction of land surface emission. If the connectivity of VOD to VWC is robust, the pair of VWC-SM observations can be viable bases for understanding soil-plant-atmosphere water relations, providing new perspectives on ecosystem science. Simultaneous SM-VOD retrievals are feasible by inverting the τ–ω model with two independent datasets in dual channel algorithms. However, given correlated satellite vertical and horizontal brightness temperatures (TB_v and TB_h), an ill-posed inverse problem arises and leads to noisy (non-robust) SM-VOD retrievals. In this study, we apply the Degrees-of-Information (DoI) metric and propose a Signal-to-Noise Ratio (SNR) metric to assess the "retrievability" of VOD given the SMAP TB_v-TB_h linear dependence. The application of these metrics allows determining where the VOD retrievals are robust and reliable. This is a necessary step in supporting applications of VOD in ecology and hydrology. Results show that regions with mainly non-woody vegetation have the best potential for VOD retrievals, though regularization is necessary. We then assess VOD time variations from two regularization products that reduce the impact of under-determined inversions: the DCA and the MTDCA, which constrain VOD time dynamics with and without using a priori VOD climatology, respectively. Though they both reduce noise, especially in the VOD retrievals, they result in differences in VOD seasonal amplitude and coupling to SM at high frequencies as we outline here.**

***Index Terms*— VOD robustness, soil moisture, regularization, microwave retrieval algorithms, SMAP.**

This work was supported by the NASA (Grant 1510842). D. Chaparro was supported by the "la Caixa" Foundation (ID 100010434) under Grant LCF/PR/MIT19/51840001 (MIT-Spain Seed Fund), by the XXXIII Ramón Areces Postdoctoral Fellowship, and by grants PID2020-114623RB-C32 and MDM-2016-0600 funded by MCIN/AEI/10.13039/501100011033 and the European Regional Development Fund (ERDF). A.F. Feldman was supported by the NASA Postdoctoral Program at the NASA Goddard Space Flight Center, administered by Universities Space Research Association under contract with NASA. (Corresponding author: David Chaparro.)

D. Chaparro is with the German Aerospace Center, Microwaves and Radar Institute, 82234 Wessling, Germany, and with CommSensLab, UPC/IEEC, 08034 Barcelona, Spain. Email: david.chaparrodanon@dlr.de.

A.F. Feldman is with the NASA Postdoctoral Program at the Biospheric Sciences Laboratory, NASA Goddard Space Flight Center, Greenbelt, MD 20771, USA. Email: afeld24@mit.edu.

M.J. Chaubell and Simon H. Yueh are with the Jet Propulsion Laboratory, California Institute of Technology, Pasadena, CA 91109, United States. Emails: mario.j.chaubell@jpl.nasa.gov; simon.h.yueh@jpl.nasa.gov.

D. Entekhabi is with the Civil and Environmental Engineering, Massachusetts Institute of Technology, Cambridge, MA 02139 USA. Email: darae@mit.edu.

I. Introduction

MICROWAVE RADIOMETERS on board the Soil Moisture Active-Passive (SMAP; launched in 2015; [1]) and Soil Moisture and Ocean Salinity (SMOS; launched in 2009; [2]) satellites measure the Earth's microwave surface emission at a low frequency (L-band; 1.4 GHz). Over land, such measurements are sensitive to the rough surface reflectivity and to the attenuation and scattering that the entire vegetation canopy exerts over the surface emission. The rough surface reflectivity is related to the soil dielectric constant and electromagnetic roughness. The inversion of estimated surface reflectivity results in estimates of surface soil moisture (SM). A byproduct of the retrieval is the amount of vegetation attenuation and scattering which together are captured by the vegetation optical depth (VOD). VOD is known to be related to the vegetation water content (VWC), the vegetation biomass, and the plants' structure ([3]–[5]).

SM and VOD are valuable hydrologic and ecological indicators important for a breadth of applications and studies. These include biomass estimation (e.g., [6]–[8]), crop yield assessment ([9], [10]), development of drought indicators (e.g., [11]), and analyses of water exchange in the soil-plant-atmosphere continuum ([12]–[14]).

The estimates of global SM fields based on SMAP and SMOS L-band measurements are routinely assessed against widely available in-situ soil moisture probe measurements. In contrast, it is less clear how well VOD represents in-situ plant physiology and phenology. Studies of how well VOD represents VWC at the satellite scale are becoming more prevalent ([4], [5], [15]–[17]). These assessments are based on sparse tower measurements and crop models which are highly informative. However, VOD in-situ measurements are sparse, leaving only limited or indirect methods for global assessment. Thus, there is still a need to determine where and to what degree VOD is more robust to satellite measurement error. The concern arises from the retrieval of two parameters (VOD and SM) from two measurements (polarized brightness temperatures) that are correlated ([18]).

To retrieve simultaneously SM and VOD, the inversion of a zeroth-order radiative transfer model (the τ–ω model; [19]) is commonly applied. This requires at least two independent sources of information in order to minimize the cost function that links measured and estimated brightness temperatures (TBs) to retrieve the appropriate SM-VOD pairs. Different approaches are considered depending on each sensor and algorithm. For the SMOS satellite, its multi-angular and dual-polarization configuration allows obtaining SM and VOD simultaneously without need of ancillary information. For SMAP, with one incidence angle (θ=40°), VOD is derived from ancillary information in order to retrieve SM when only one polarization is used (i.e., the Single Channel Algorithm; SCA; [20]). Alternatively, both horizontal and vertical polarizations are applied in the Dual Channel Algorithm (DCA) to simultaneously retrieve SM and VOD ([21]). Nevertheless, these TBs at horizontal (TB_h) and vertical (TB_v) polarizations are often correlated, containing redundant information ([22]) and thus not being independent measurements. As a result, DCA approaches are ill-posed and can lead to difficulty in algorithmic gradient search methods finding the true SM and VOD values for a given snapshot ([23]).

The underdetermination of the VOD and SM inversion due to correlated polarization measurements is expected to introduce noise into the retrievals. We expect that the noise has different characteristics at different frequencies. At longer time scales such as the seasonal cycle, we expect that the various approaches to regularize the inversion yield similar results. Indeed, [24], [25] and [26] show that the seasonal cycles of the various approaches are similar and the climatologies of VOD are comparable. Our concern, however, is that the noise at the much higher frequencies such as the overpass-to-overpass or the Nyquist frequency may be at different levels depending on the approach to the inversion. This would impact studies that examine short-time scale (i.e., sub-weekly to monthly) covariations in VOD and SM, such as the study of the soil-plant-atmosphere water dynamics. Most other studies that examine climatologies of VOD (e.g., those focusing on above-ground biomass, crop phenology, etc.) may be less affected.

In order to quantify how well-posed the inversion is, previous work estimates the Degrees of Information (DoI) metric (DoI is defined in [18], and measures the fractional amount of information, which is between 1 and 2 in a pair of measurements). Because TB_v and TB_h as observation pairs are correlated, DoI is below 2. Hence, retrievals of SM and VOD by using two polarizations are not fully independent and errors can potentially affect one or both retrievals. The spurious noise reduces the robustness of the method ([18] and [27]). For multiple angles, this effect is expected to be less pronounced due to the higher amount of information available ([28], [29]), although the depolarization with more dense vegetation will still reduce the amount of information across the angles.

To overcome this issue, SMAP-based VOD-SM retrievals have introduced various regularization approaches that aim to reduce retrieval noise by incorporating a priori information mainly about variations in VOD. The Multi-Temporal Dual Channel Algorithm (MTDCA) is based on the premise that changes in the vegetation biomass occur on time scales that are longer than soil moisture fluctuations due to storms and inter-storms ([27], [30]). Based on this assumption, the MTDCA uses two consecutive overpasses to retrieve two soil moisture values and a single VOD output for each time-adjacent overpass pair. It also uses model-selection over the entire record to estimate the effective single-scattering albedo as a static feature of the dominant vegetation type. Hence, four TB values (two for each overpass) are available to retrieve three unknowns. This increases DoI above three ([27], [31]). As DoI is the upper limit on the number of possibly retrieved parameters, the problem is not necessarily overdetermined. This procedure results in two VOD values retrieved for each overpass (one using information from the overpass before and one using information from the overpass after). In averaging these two VOD values together, information from multiple overpasses ultimately constrains the VOD retrieved at a given overpass. Recently, other algorithms have also included time aggregation with a priori decision of the degree of regularization: the SMOS L3 algorithm ([32]) and the Constrained Multi-Channel Algorithm (CMCA; [23]). These approaches often incorporate a penalty on time rates of change of VOD ([24], [33]). Following a similar concept, new SMAP L3 Dual-Channel Algorithm retrievals (also known as DCA; [21], [34]) incorporate a Tikhonov regularization ([35, p.]). This approach instead imposes a weighted a priori VOD based on MODIS Normalized Difference Vegetation Index (NDVI) and penalizes deviations of the SMAP-retrieved VOD from this assumed time series. The retrieved VOD is therefore constrained by a less noisy, NDVI-based VOD seasonal climatology ([21]).

Despite these advances on new information metrics and regularization techniques, SMAP dual-channel algorithms and regularization approaches still need to be evaluated. We recognize that the DoI metric is useful to quantify the information available in satellite measurements, but it does not uniquely indicate robustness of the retrievals. For example, DoI may increase with more random noise (i.e., independent TB_v and TB_h values), which paradoxically suggests more robustness to noise. Therefore, here we introduce an additional metric of retrieval susceptibility to noise (and hence robustness): the Signal-to-Noise Ratio (SNR). It complements DoI in order to provide a holistic understanding of the VOD retrieval algorithm robustness.

Regularization techniques can over-constrain the resulting VOD, thus removing VOD variability that contains a physical signal and creating an unwanted smoothing effect ([24], [25]). We examine VOD from two common regularization techniques (Tikhonov for DCA, and multi-temporal for MTDCA) at different time scales in order to gain an understanding of error sources and characteristics. Note that DCA, hereafter, refers to regularization of VOD with the Tikhonov regularization and not DCA in the traditional sense of a simultaneous inversion to obtain soil moisture and VOD without regularization. Figure 1 shows examples that motivate this research. It shows time-series of VOD from MTDCA and from DCA in several different vegetation conditions. In low vegetation (grasslands), both VOD products have similar patterns in terms of variability (Figure 1a). Figure 1b shows that seasonal variations in a woody savannah are captured by both approaches, but with a smaller DCA seasonal amplitude. We aim to understand if either of the regularization approaches may be under or overregularizing the VOD variability both in seasonal and high-frequency variations. Figures 1c and 1d show how high-frequency MTDCA VOD variation increases with biomass (i.e.,

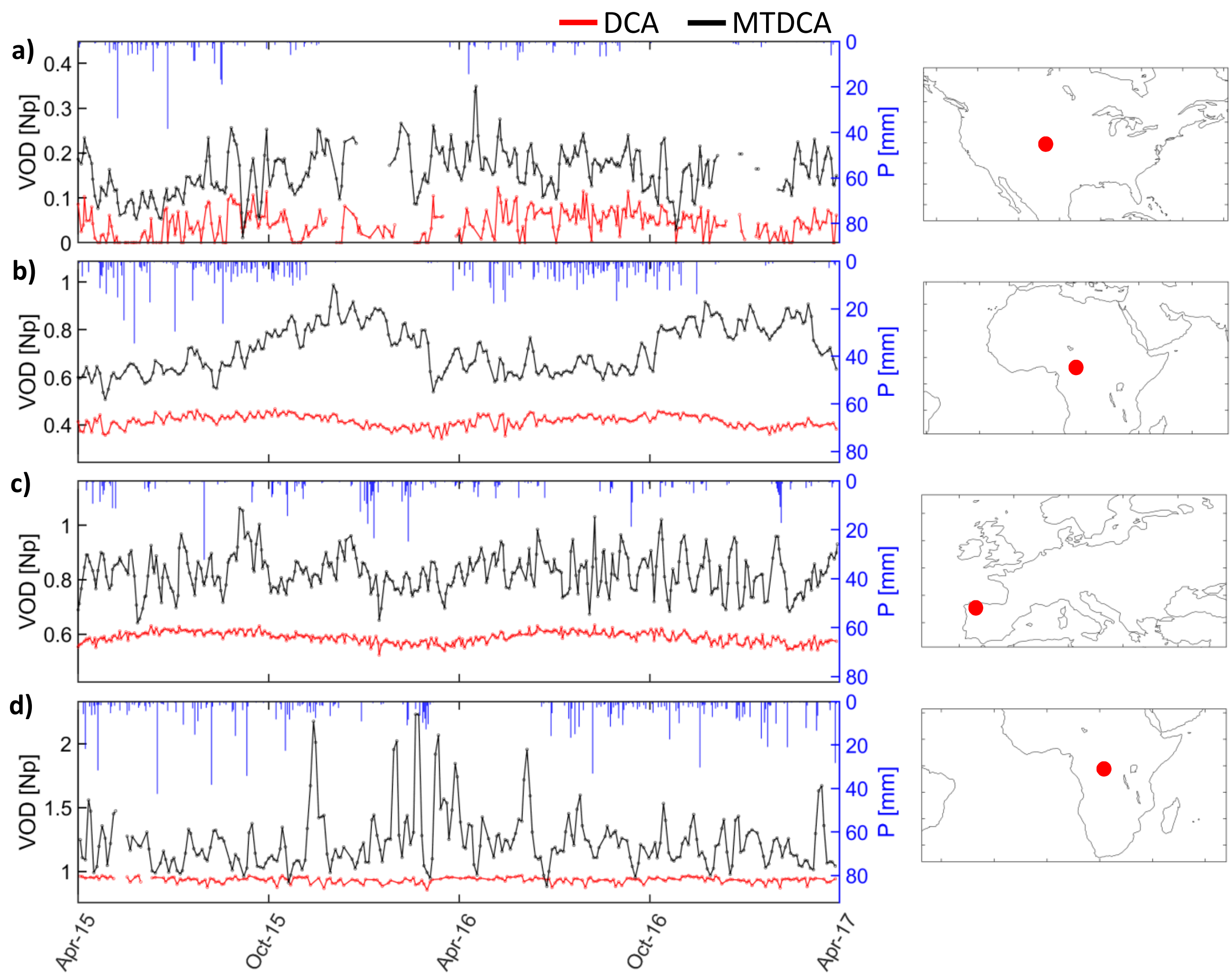

Figure 1. MTDCA VOD (black line) and DCA VOD (red line) in (a) grasslands in central North America; (b) woody savanna in the Sahel; (c) deciduous forest in the northern Iberian Peninsula; and (d) tropical forests in the Congo basin. VOD data used in this figure is detailed in Section 2.1. Precipitation estimates are based on the Global Precipitation Measurement (GPM) IMERG Final Precipitation L3 v06 product at 0.1° resolution ([36]). Off-sets between

the largest rapid changes are found in the tropical forest pixel), while the DCA VOD time-series is smooth in both cases (especially in the tropical forest). For dense vegetation, this motivates investigating whether the MTDCA approach may be carrying excess noise in its retrievals in high plant biomass regions. It also motivates determining whether the DCA is overregularizing VOD variability, creating an unintended smoothing effect.

Therefore, in this study we first assess the retrievability of VOD by examining observed TB_v- TB_h differences and using DoI and the proposed SNR. Second, we compare the VOD retrievals and noise of multi-temporal and Tikhonov regularization techniques. We perform this test for both the full signal and the high-frequency signal near the Nyquist frequency. Our driving research questions are:

- Which metrics quantify uncertainty in SM and VOD retrievals due to instrument noise and what do they reveal about current global SM-VOD retrievals?
- How do the retrieved VOD time series based on commonly used regularization approaches qualitatively compare across different timescales of variability?

This work thus complements recent efforts to determine how TB error relatively propagates into soil moisture and VOD in these algorithms, how much retrieved soil moisture and VOD error is attributed to errors in the satellite measurements, radiative transfer model, and algorithmic parameterization, as well as how much VOD regularization reduces these errors [22, 24, 25, 37].

II. Data and Methods

A. Datasets

The SMAP mission was launched by the National Aeronautics and Space Administration (NASA) in January 2015. It has a native spatial resolution of ~36 km (based on half-power or -3 dB definition) and a revisit time of approximately 2-3 days depending on latitude. The following SMAP datasets are studied globally, using the descending passes of the satellite (6 am) for the period April 2015-March 2020:

- Brightness temperatures at both vertical (TB_v) and horizontal (TB_h) polarizations from the L1C radiometer product, version 2 ([37]). This product contains calibrated, geolocated TBs derived from SMAP Level-1B (L1B) antenna temperatures. Backus-Gilbert optimal interpolation methods are applied to extract maximum information from the antenna temperatures of SMAP and convert them to TBs at 9 km gridding (EASE2 grid).

- The SMAP DCA that contains SM, VOD and constant albedo (ω) datasets. It is the SMAP enhanced L3 radiometer soil moisture product, version 4 ([39]), also at 9 km gridding. It relies on the DCA algorithm to retrieve SM and VOD from the aforementioned L1C TBs. SM and VOD retrievals in this product are based on a Tikhonov regularization approach designed to remove excess noise in the VOD estimates, but at the cost of assuming an a priori VOD time series (see Section 1). To do so, this method defines a degree of regularization which modifies the least squares misfit (χ^2) between modelled TBs (as a function of SM and VOD) and measured TBs. As such, this approach penalizes the retrieved VOD's deviation from the a priori VOD time series with the degree of penalty determined by an a priori multiplicative factor. Therefore, the regularization inputs information about VOD variations based on other time series such that the correlated TB observations can be potentially used to reliably retrieve SM and VOD with reduced noise. More details on this regularization method are provided in [21] and in [40].
- The SMAP MTDCA SM, VOD and ω datasets ([30], [41]). Note that ω is constant for the study period. The product is also derived from the SMAP L1C 9 km TBs and applies the MTDCA retrieval algorithm for two consecutive overpasses. The algorithm is based on a time-series method which uses all TB values within a predefined time window. The default window length is two overpasses (i.e., 2 to 3 days depending on latitude). VOD is held constant between the two overpasses, but this is repeated for each time-adjacent overpass pair such that information from both time-adjacent overpasses is used (averaged) in the VOD retrieval. Therefore, the VOD variations, especially those due to noise, are reduced. Ultimately, this approach penalizes large changes in VOD between overpasses, eliminating noise more than physical VOD signal [25].

In order to analyze the results, data sets on vegetation density and type are used. This includes the Vegetation Water Content (VWC) product ([34]) that is used in the Single Channel Algorithm (SCA). This VWC product is derived from NDVI seasonal climatologies from the NASA MODIS satellite for use within the SMAP algorithms. Also, land cover (LC) data from the MODIS International Geosphere-Biosphere Program (IGBP, MCD12C1 product v.6; 3 km resolution) is used to define homogeneous vegetation classes in two steps: (i) only the fully homogeneous 9-km pixels (i.e., those containing all 3-km pixels of the same LC class) are considered; (ii) latitude and homogeneous land cover pixels are applied to define seven different vegetation classes (Table S1). In addition, note that IGBP LC has been used to screen out barren and snow-ice regions in the analyses.

B. The τ–ω framework and reliance on TB polarization differences

Retrievals of SM and VOD from passive microwave measurements rely on the inversion of a “zeroth order” radiative transfer model, commonly known as the τ−ω model ([19]). In this model, the L-band brightness temperatures (TBs) are represented as the sum of three terms: (i) the upwelling vegetation emission, (ii) the downwelling emission from vegetation, which is reflected by the soil and then attenuated by the canopy, and (iii) the direct soil emission and its attenuation through the vegetation:

$$TB_p = (1-\omega)(1-\gamma)T_c + (1-\omega)(1-\gamma)\gamma \cdot r_p \cdot T_c + (1-r_p)\gamma \cdot T_s \quad (1),$$

where γ is the vegetation transmissivity, which depends on the vegetation optical depth (VOD; algebraically represented by τ) according to the Beer's law:

$$\gamma = e^{(-\frac{\tau}{cos\theta})} \quad (2),$$

where θ is the incidence angle. Then, τ (used synonymously with VOD here) is one of the two unknowns to be retrieved. The VOD can be different for different polarizations. However, currently, neither the SMOS nor the SMAP science data products account for any polarization difference; both assume VOD is the same at both polarizations due to mixed orientation of vegetation at the 36 km scale. The soil reflectivity at polarization p (r_p) is linked to the soil dielectric constant through Fresnel equations and a nominal value of isotropic soil roughness. The soil dielectric constant is dependent on soil texture and soil moisture. SM is the other unknown to be retrieved in the τ-ω framework. The effective scattering albedo (ω) accounts for extinction and scattering effects due to vegetation. Albedo is obtained from nominal values distinguishing forest/non-forest vegetation in the case of the SMOS current algorithms ([42, p. 2]) and from look-up tables based on land cover in the case of the SMAP ones (e.g., [34]). Like VOD, the albedo can have polarization differences that are not considered at this time. While efforts are underway to understand ω and its time dynamics ([43]), we focus only on SM and VOD retrievability here. T_c and T_s are the temperatures of the canopy and the soil, respectively. Both temperatures are assumed to be equivalent at SMOS and SMAP overpasses times (6 am and 6 pm local times) and are obtained from ancillary surface temperature information. The isothermal assumption is known to hold well near 6 am local time.

In dual-polarization algorithms, theoretically VOD may be inferred alongside SM if there is observed TB polarization-dependence above instrument noise. This is shown when separating out the polarization dependent term (r_p) from (1):

$$\frac{TB_p}{T} = \gamma + (1-\omega)\cdot(1-\gamma) + \gamma r_p[(1-\omega)\cdot(1-\gamma) - 1] \quad (3),$$

where the two values of surface reflectivity (r_p; one for TB_v and one for TB_h) will lead to two equations. In (3), the first term is the same for both polarizations (in the SMAP and SMOS implementations) and only the second term adds any polarization difference in the forward model. The joint retrievability of SM and VOD depends on a large enough difference in TB measurements at H and V polarizations. VOD is part of γ (see (2)). If TB_v and TB_h approach one another, this suggests that the differences in r_h and r_v values are not making a large contribution to the emission as surface reflectivity typically has large differences at H and V polarizations. In this scenario, TB measurements have less contribution from the surface emission influenced terms in the final bracketed term in (3) and thus only VOD can be retrieved. However, this results in optimization instability when still attempting joint retrievals under this scenario (many combinations of possible SM and VOD would satisfy (3)). Therefore, the robustness of dual-channel algorithms is highly affected by the brightness temperature polarization difference fluctuations close to the instrument noise level, which can create noise in the estimations.

C. *Analysis of the VOD retrievability*

To assess the VOD robustness, first the relationship and differences between TB_h and TB_v are evaluated for different bins of VWC: 0 to 1 kg/m^2, 3 to 4 kg/m^2 and >9 kg/m^2. They represent three contrasting classes of vegetation density, ordered from lower to higher VWC (i.e., from lower to greater biomass): (i) low vegetation in semi-arid regions, tundra, and steppes; (ii) woodlands and non-tropical forests; and (iii) tropical forests (Figure S1). This first analysis provides the broader context which addresses how vegetation types reduce the TB_v – TB_h differences and, quantitatively, how close are they to the instrument noise.

Second, we use the Degrees of Information (DoI) as proposed in [18]. DoI is a measure of how much independent information exists in several measurements (for example, TB_v and TB_h) when the measurements are correlated. DoI is computed as:

$$DoI = N - C_n(X_1, \dots, X_n) \quad (4),$$

where N is the number of parameters (here, N=2 if considering a single snapshot with TB_v and TB_h) and C_n represents the total correlation among the different parameters X_1 to X_n (here, TB_v and TB_h). The total correlation is a generalization of the mutual information which consists of the Kullback–Leibler divergence between the joint and the marginal entropies of the datasets. C_n captures the amount of information shared between any of the measurements in a set ([18], [44]). Higher total correlation suggests less independent information between two parameters.

Third, we introduce a Signal-to-Noise Ratio (SNR) metric to quantitatively assess retrievability. It measures how much TB_v and TB_h (two correlated measurements) are different relative to the instrument noise. The dispersion (standard deviation) of the polarization difference relative to the TB_v-TB_h linear dependence is computed. In Figure 2, this polarization difference is distance L and is represented by solid red lines.

Once σ(L) is obtained, then the SNR metric is

$$SNR = \frac{\sigma^2(L)}{(NEDT_v^2 + NEDT_h^2)} \quad (5),$$

where NEDT states for Noise Equivalent Delta Temperature for the L1C TBs, which is the measurement of the instrument noise. NEDT equals 0.77 according to the L1C TBs Assessment Report ([43]; p. 43). The value is estimated over a stable vicarious target or constant temperature and salinity ocean patches. Here, NEDT of vertical and horizontal polarizations are assumed to be independent.

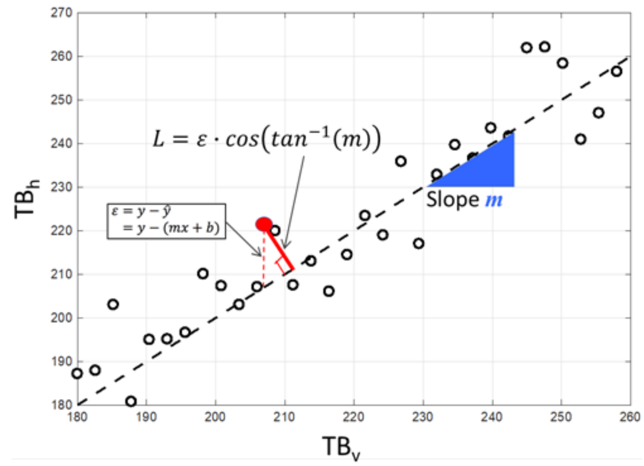

Figure 2. Graphical summary of how the difference relative to the TB_v-TB_h linear dependence (L; solid red line) is computed.

D. *Metrics to interpret the effect of regularization on VOD and noise*

Regularization techniques can mitigate issues of correlated TB_v and TB_h measurements. However, there are different regularization approaches that have produced satellite VOD retrievals and their differences have not been assessed. The SMAP DCA VOD uses the Tikhonov regularization:

$$\min_{X=VOD,SM} J = \sum_{p=H,V} \left(TB_{p\,Obs}(X) - TB_{p\,Mod}\right)^2 + \lambda^2 \left(VOD_t - VOD_{prior_t}\right)^2 \quad (6),$$

where for a given overpass, VOD is retrieved simultaneously as in the traditional DCA (first addend), but a penalty (λ) is placed on VOD deviations from a prior input VOD based on NDVI climatology (second addend). This VOD prior input was previously used in the SMAP single channel algorithm soil moisture retrievals. A larger λ value would force the retrieved VOD to be closer to the VOD prior. By contrast, the MTDCA uses time adjacent overpasses assuming that VOD is constant between n overpasses (n=2 in the studied product; see Section 2.1).

$$\min_{X=VOD,SM_1,SM_2} J = \sum_{t=1}^{n=2} \sum_{p=H,V} \left(TB_{p\,Obs}(X) - TB_{p\,Mod}\right)^2 \quad (7),$$

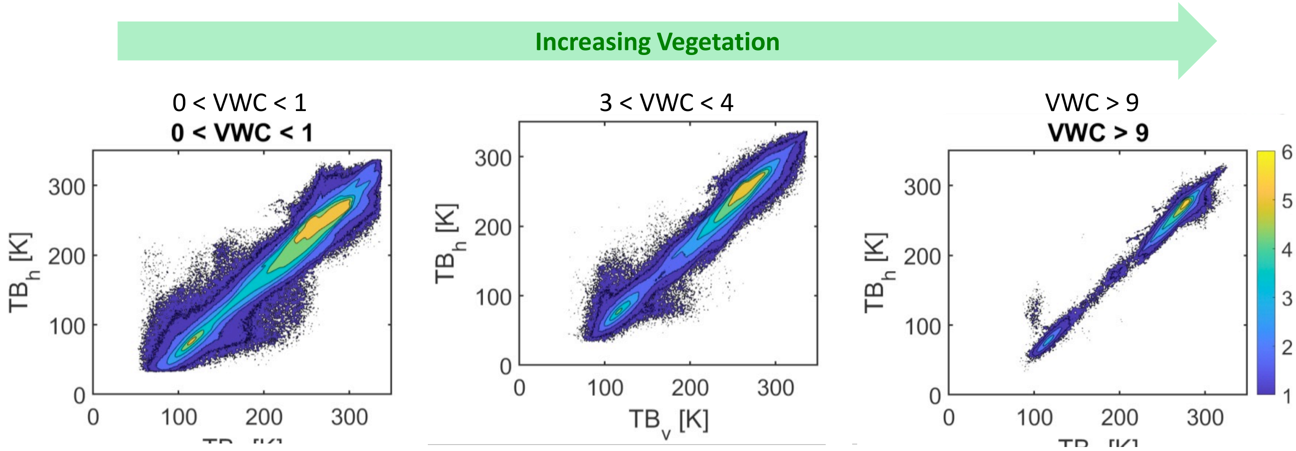

Figure 3. Comparison of SMAP brightness temperatures at vertical (TB_v; x-axis) and horizontal (TB_h; y-axis) polarizations for increasing Vegetation Water Content (VWC): 0-1 kg/m2 (left); 3-4 kg/m2 (center); and >9 kg/m2 (right). See Figure S1 for a map of the global distribution of the three categories. The color bar shows the density of pixels (decimal logarithm of the number of pixels).

To evaluate the impacts of multi-temporal and Tikhonov regularizations on the resulting VOD and noise, both the MTDCA and the DCA products will be assessed and compared at different time scales. Results will be interpreted in the context of DoI and SNR. First, the mean annual VOD and the seasonal amplitude of the raw VOD signal are estimated and compared between the products. Second, the near-Nyquist frequency of VOD (NyVOD) and SM (NySM) will be computed by subtracting the 7-day moving averages from both raw variables. The high-frequency changes in VOD will be analyzed by means of the standard deviation of the NyVOD. This will provide insight into the amount of remaining high-frequency VOD variations after regularization. Third, the covariance between NyVOD and NySM will be calculated in order to understand the influence of SM-VOD compensation occurring with noisy inputs during inversion and differences in this coupling between the two products. These results will be discussed in the context of SNR and SM-VOD retrieval errors compensation.

Note that VOD differences between algorithms will not solely be a function of the differences in regularization approaches in (7) and (8) because both approaches have different algorithmic choices, mainly in scattering albedo and roughness parameters. Though we aim to address our second research question focusing on the aforementioned regularizations (which are commonly used in VOD studies), we also conduct complementary analyses on the impact of different albedos in the VOD differences between algorithms. In addition, we discuss the role that roughness may have on these differences.

III. Retrievability of VOD according to DoI and SNR metrics

The capacity of the τ-ω framework to provide accurate VOD retrievals depends on the availability of at least two independent pieces of information. However, Figure 3 shows that TB_v and TB_h are highly correlated. Indeed, the TB_v – TB_h difference narrows as VWC increases (see (2) and (3)). In the densest

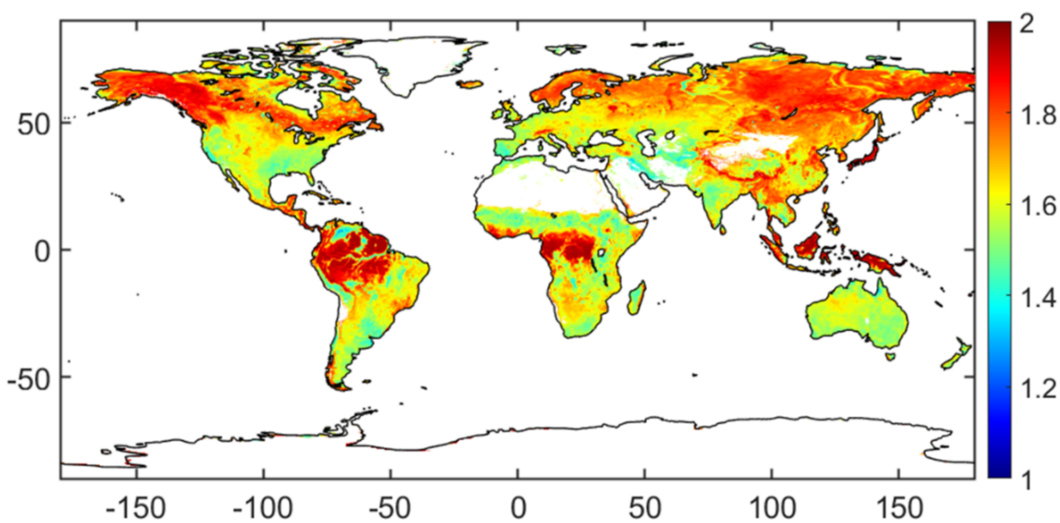

Figure 4. Degrees-Of-Information (DoI) for brightness temperatures at vertical (TB_v) and horizontal (TB_h) polarizations. DoI measures how much independent information exists in several measurements (here two) when they are correlated (e.g., DoI = 1.5 indicates that 1.5 parameters may be retrieved).

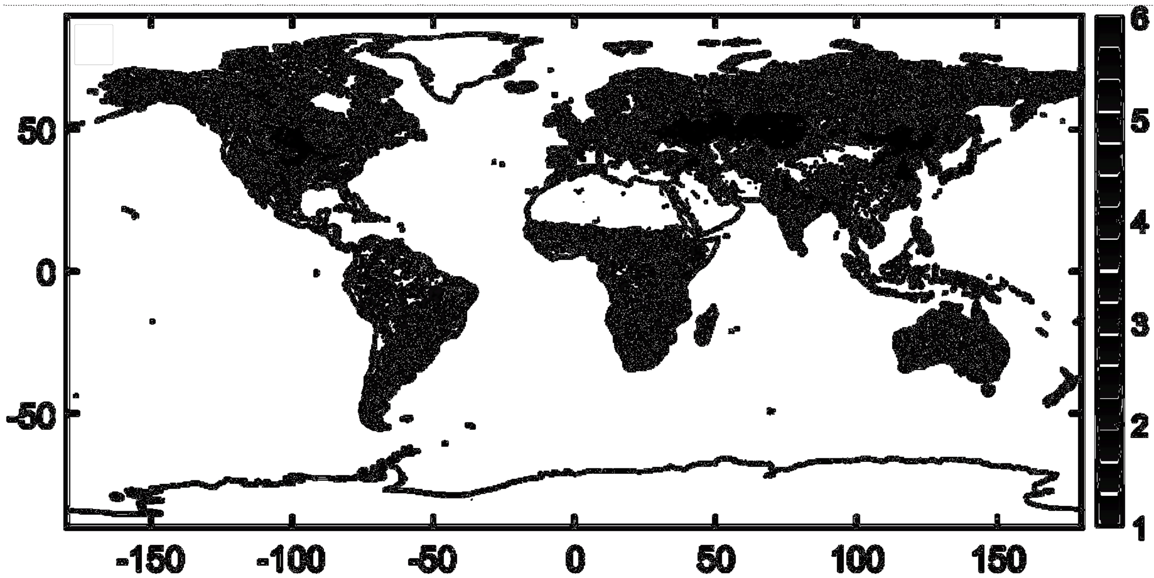

Figure 5. Map of Signal-to-Noise Ratio (SNR), which is based on σ(L). SNR provides is a new metric to evaluate the robustness of VOD retrievals.

canopies where VWC > 9 kg/m^2 (i.e., tropical forests; Figure S1) the differences and their variability become small. This illustrates why TB_v and TB_h do not represent two independent data sources (Figure 3). In contrast, regions with less vegetation density (VWC<1; i.e., semi-arid regions; Figure S1), do show larger differences and variations between vertical and horizontal polarizations (Figure 3). This eases the partitioning between soil moisture and VOD in the retrieval approaches as demonstrated with (3).

The DoI metric can be used to quantify the amount of independent information in the two measurements. Figure 4 shows the DoI map where, generally, DoI ranges between 1.5 and 1.8 for two polarizations in many regions. Hence, theoretically, around 1.5 parameters can be inferred with a single satellite overpass (i.e., there is approximately 1.5 independent information content in TB_v and TB_h). In the case of multi-temporal retrievals, the number of parameters that can be inferred should be (theoretically) the result of multiplying DoI by the number of overpasses (e.g., roughly three parameters for two consecutive samples; [27]).

Nevertheless, DoI needs to be interpreted with caution as it may give "false positives" in very dense canopies if it is not interpreted in the context of noise. In particular, Figures 4 and S2 show that DoI is very close to 2 in dense tropical forests (i.e., the Amazon, the Congo basin and Indonesia). This is because

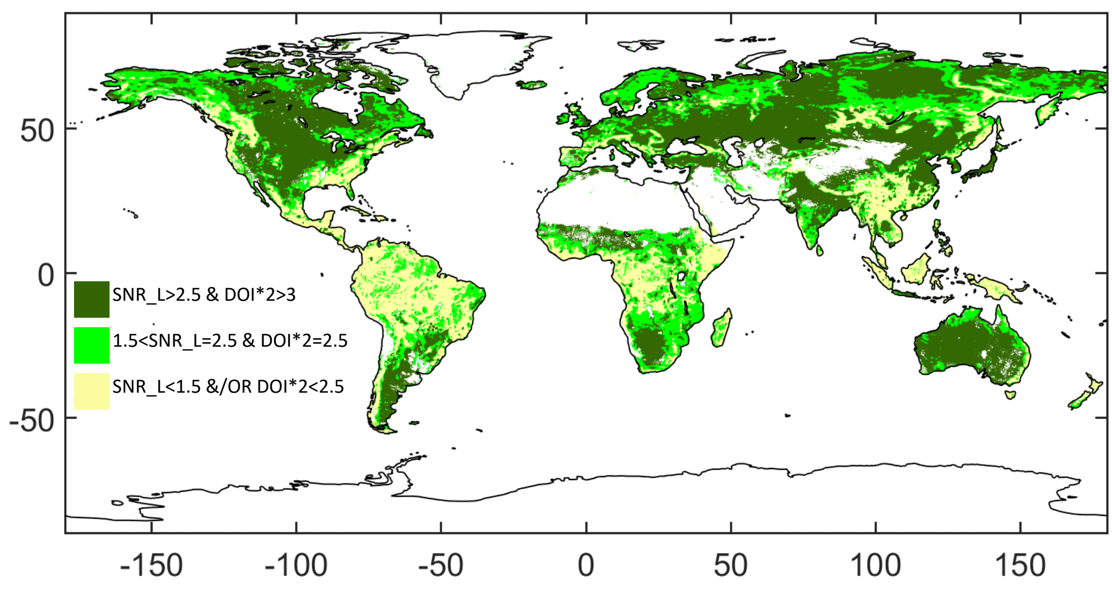

Figure 6. Uncertainty of joint SM and VOD retrievals with regularization based on SNR and DOI. Dark green (higher confidence) spans through 44.2% of global vegetated land, light green (medium confidence) through 27.3%, and light yellow (lower confidence) through 28.5%.

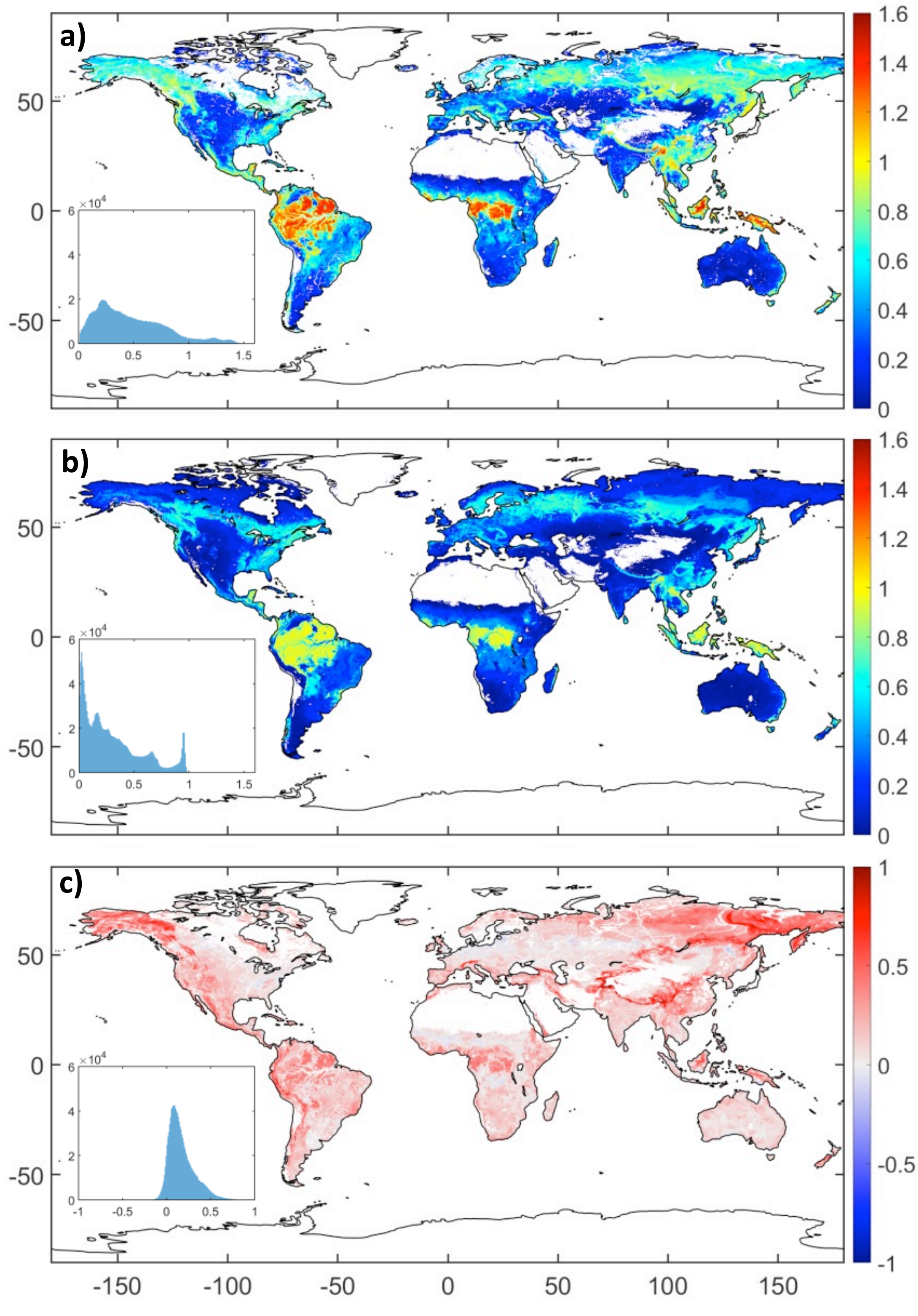

Figure 7. (a) Mean of VOD retrieved with MTDCA; (b) mean of VOD retrieved with DCA; (c) differences between both VOD retrievals (MTDCA – DCA).

noise dominates the signal in these dense vegetation regions. Variations in brightness temperatures are small or comparable to instrument noise. Hence, DoI is essentially measuring the independence of two uncorrelated time series. It suggests there is enough independent information to retrieve two unknowns but does not consider that the variations are dominated by instrument noise rather than physical signal. This results in a deceiving DOI value of 2 for the pair. The polarization due to surface reflectivity (3) is largely attenuated: TBs are depolarized (Figure 3), suggesting that only the instrument noise might be present in the measurements.

Thus, there is a need for an additional signal-to-noise ratio

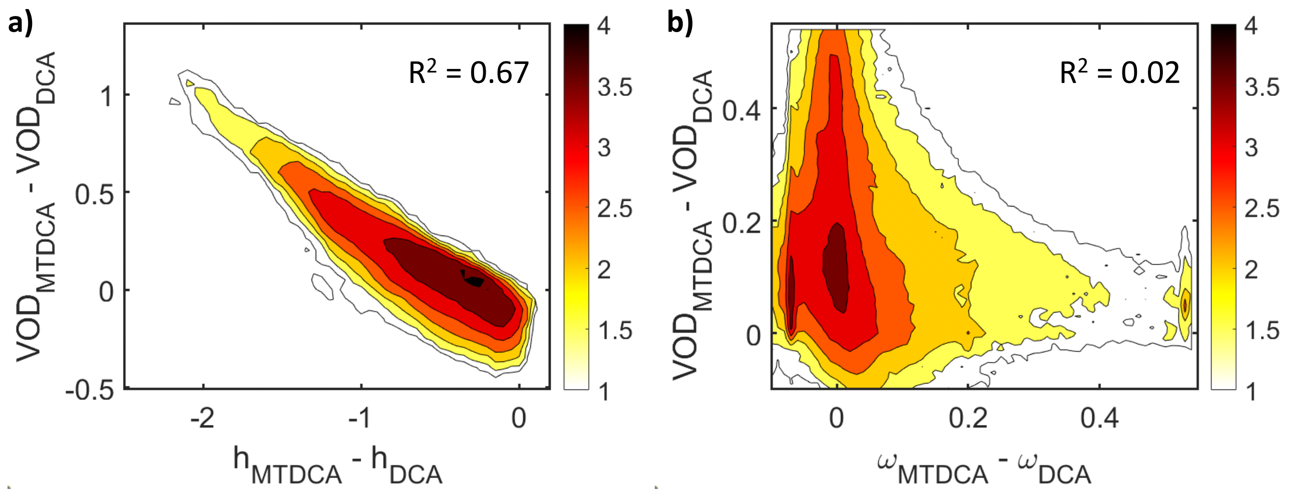

Figure 8. Differences in VOD climatology between algorithms are compared to (a) differences between algorithm roughness parameter (h) and (b) differences in albedo (ω). The colorbars show logarithm of counts. Roughness parameter differences explain nearly 70% of the mean bias in VOD from each algorithm. The scattering albedo has only minor impact.

metric to interpret the retrievability where the fluctuations in brightness temperature approach the instrument noise level. We introduce a SNR metric to complement the DoI in interpreting VOD retrievability. The SNR should measure, in the context of instrument noise, the ratio of signal to noise present after linearly predicting one covariate from another.

Figure 5 shows the map of SNR. SNR values are close to 1 in dense tropical forests (median SNR = 1.24). This indicates that the signal is greatly influenced by noise and suggests caution in interpreting DoI alone. A low SNR shows that DoI is likely only higher in tropical forests because the total correlation is low due to noise. This quantifies the problem and shows, geographically precise, where retrievals of VOD may be problematic (Figures 4 and 5). In other forest types, as well as in savannas, the value of DoI decreases and the SNR increases as compared to tropical forests (median DoI and SNR in temperate forests: 1.72 and 1.44, respectively; median DoI and SNR in savannas: 1.60 and 1.71, respectively; Figure S2). In the case of boreal forests, a higher SNR is found (median SNR = 2.24). Overall, this shows that VOD and SM retrievals based in dual-channel algorithms should be robust in terms of available information in most land regions including non-tropical forests.

In contrast, lightly vegetated, non-forested regions have the largest variations in the difference in horizontal and vertical polarization TBs (Figure 3). As shown in Figures 5 and S2, this results in SNR values over 3 in semiarid regions (e.g., the Sahel and central Australia), grasslands (e.g., Central Asia, the US Great Plains and the Pampas), and croplands (e.g., the US Corn Belt, Ukraine, Argentina and the SW and SE areas of Australia). In these areas, the low vegetation density permits a good retrievability with high SNR, but in need of regularization as shown by DoI values closer to 1.5 (Figures 4 and S2). Hence, VOD and SM retrievals will be achievable where DoI and SNR are both high. However, based on these SMAP measurements, DOI is well below 2 where SNR is high meaning that some degree of regularization is needed to stabilize retrievals. DoI can be adjusted with regularization. However, SNR is intrinsic to the satellite measurements and thus cannot be directly altered. Therefore, we anticipate retrieval difficulty of VOD in wooded regions with low SNR, but an improvement on VOD retrievals after regularization in grasslands, croplands and shrublands as well as in few cases of boreal and temperate forest areas (Figures 6 and S2).

Taken together, DoI and SNR metrics suggest that VOD can be robustly retrieved with regularization in regions with low and moderate vegetation density with an increase in uncertainty in most savannas and forests, especially in tropical ones (Figure 6). If DoI is doubled in a regularization approach (see Section 4), in regions where SNR is also high, both SM and VOD can be retrieved with lower risk of estimation instability within the optimization (Figure 6). Figure 6 should be used as a guide in determining where dual retrievals of SM and VOD are most certain using regularization approaches.

IV. Impacts of Tikhonov and Multi-Temporal Regularizations on VOD Retrievals and Noise

Global patterns of time-mean total VOD signal are shown in Figure 7 for MTDCA (multitemporal regularization) and DCA (Tikhonov regularization). The spatial patterns are similar, with Pearson's correlation coefficient (r) equal to 0.89, although mean VOD values for MTDCA are generally higher than those for DCA (Figure 7). These differences are partially attributable to choices of the roughness parameter (*h*) in both algorithms, where higher *h* inputs generally reduce mean VOD. In particular, differences in *h* explain 67% of variance of the difference between the average VODs of both products (Figure 8a), where lower DCA's mean VOD can be partially explained by its higher *h* inputs. Again, note that the DCA here includes the SMAP product with Tikhonov regularization and is not a traditional DCA snapshot retrieval. In addition, note that we have found no relationship between differences in average VOD and those in ω (Figure 8b).

The components of VOD variability at low frequency (i.e., seasonal amplitude) are shown in Figure 9. Note that since the DCA is constrained by NDVI climatology, the seasonal

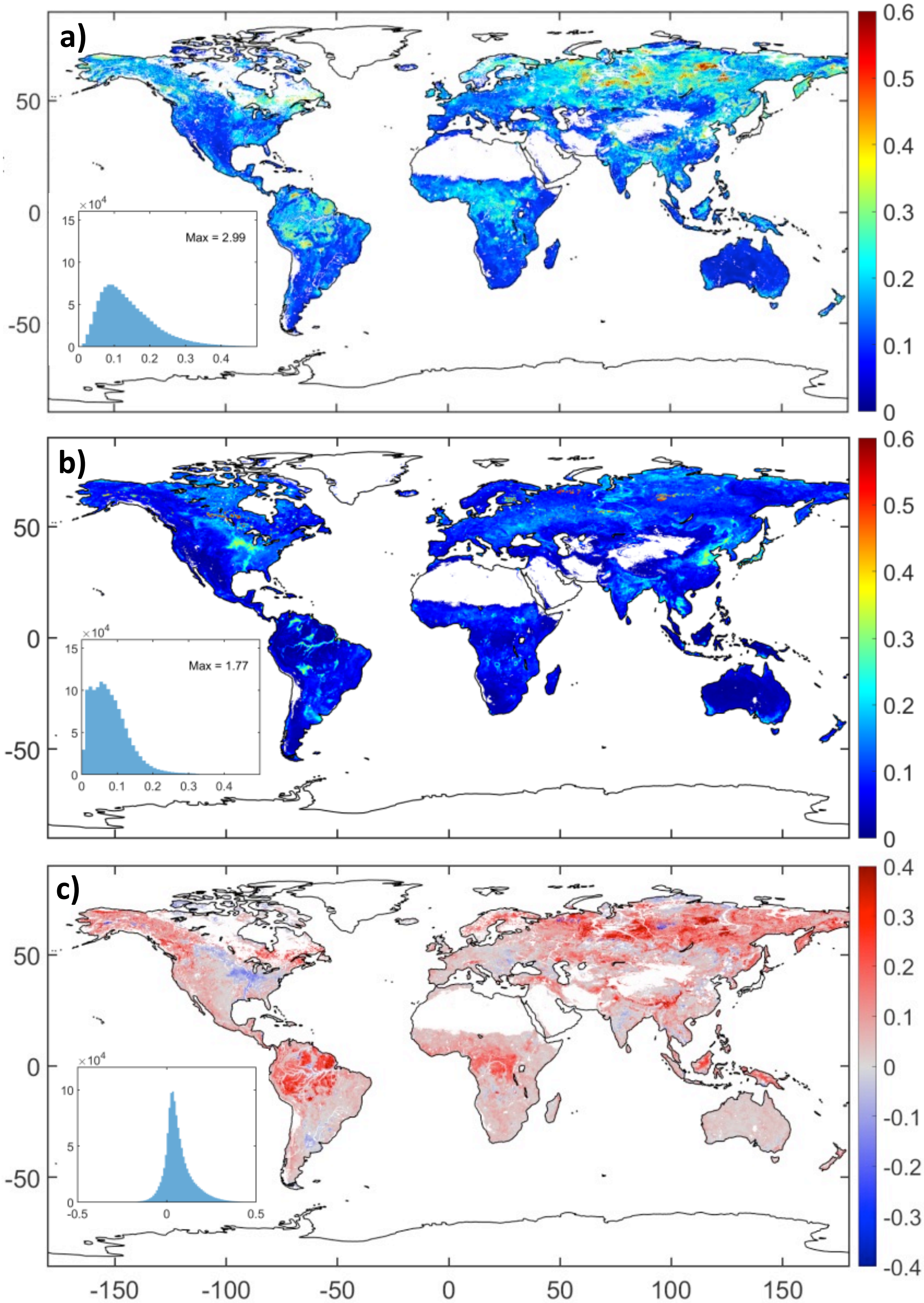

Figure 9. Seasonal amplitudes of (a) MTDCA VOD and (b) DCA VOD; (c) differences between seasonal amplitudes (MTDCA – DCA).

amplitude may partially be driven by the NDVI climatology amplitude and/or spatial pattern of conversion factors to VOD. The seasonal amplitudes are broadly comparable (r=0.44), but the MTDCA shows slightly higher amplitudes, especially in forests (Figure 9c). This is expected because (i) the DCA's NDVI climatology prior will suppress any VOD interannual variability, and (ii) NDVI signal saturates for closed canopies and more dense vegetation ([45]), thus placing a maximum on the NDVI-based climatology used in DCA regularization. We suggest that these considerations may be dampening the seasonal amplitude of DCA VOD. A particular exception is croplands, where the seasonal amplitude is larger for the DCA

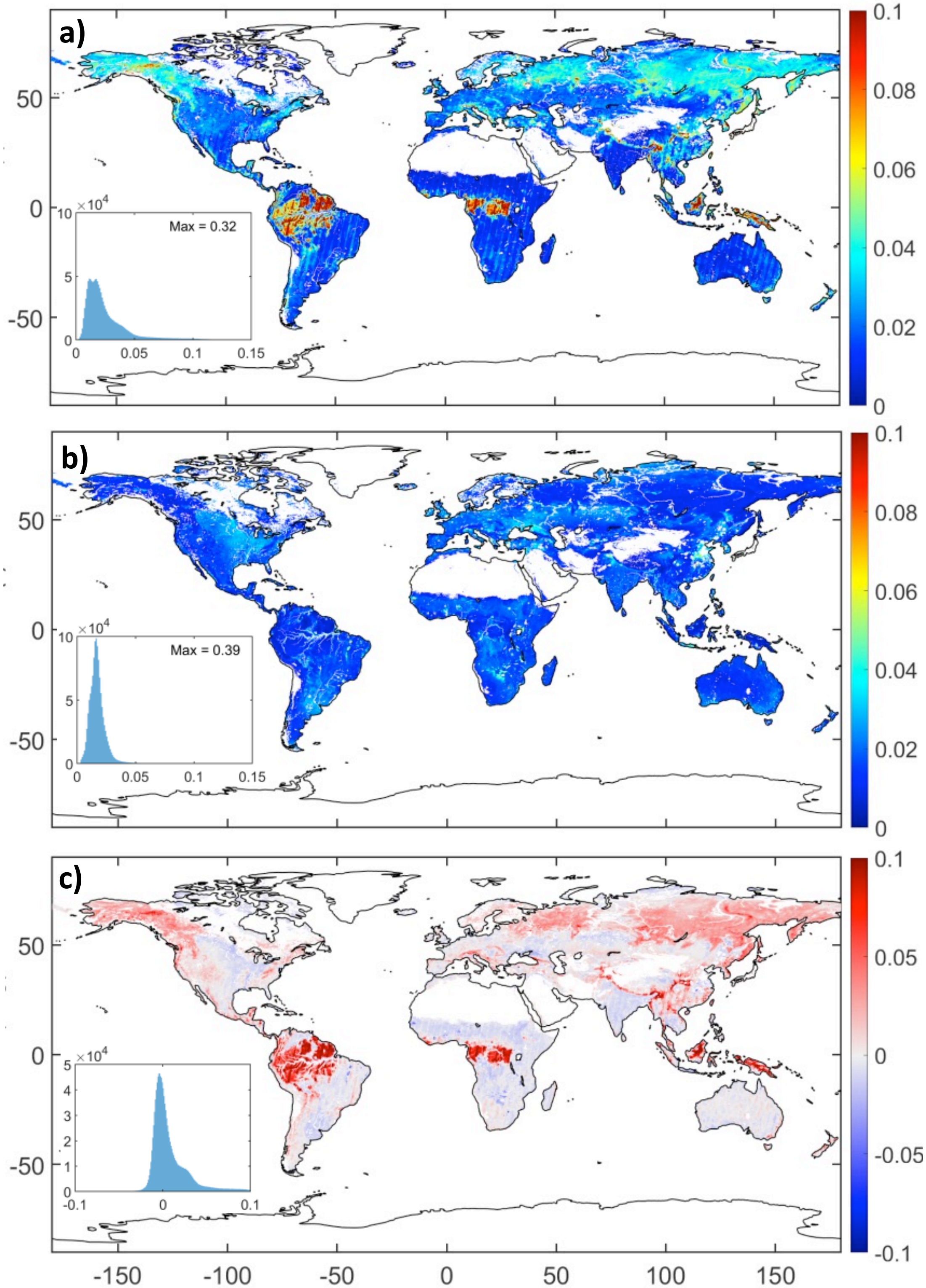

Figure 10. Standard deviation of VOD at the Nyquist frequency for (a) MTDCA and (b) DCA; (c) The MTDCA minus the DCA VOD standard deviation at the Nyquist frequency. In the inset, Md is the median and Mn is the mean.

product than for MTDCA. This is evident in the US Corn Belt and in crop areas of Argentina (Figure 9c). We suggest that time-based regularization approaches without a prior (like the MTDCA) may have reduced capacity to capture the rapid growing phase seasonality and sharp amplitude in these regions; rapid corn growth may cause large VOD changes (around 0.2 Np) in less than 10 days that VOD regularization approaches will dampen ([33]).

Overall, the difference in seasonal amplitudes may originate from both regularization approach differences as well as other parameter choices. For example, the magnitude of effective single-scattering albedo (ω) scales the impact of VOD on the

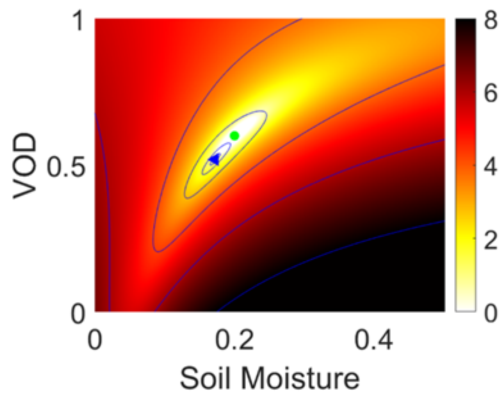

Figure 11. Dual-channel algorithm estimation cost function using synthetic data. The blue symbol is the true solution while the green symbol is the noisy solution when TB error on order of 1 K is added to the measurements. Adapted from Figure 1 in Konings et al., 2016.

brightness temperature. However, we find that these seasonal amplitude differences are not linked to changes in ω between algorithms (results not shown) consistently with differences in mean VOD not being linked to changes in ω neither (Figure 8b). Instead, similarly to the differences in VOD time means, a generally larger h roughness parameter chosen for the DCA (Figure 8a) and the use of an NDVI-based seasonality likely contribute to decrease the DCA VOD seasonal variability in comparison to that of MTDCA.

We now evaluate the higher frequency variability near the Nyquist frequency (periods of 4-7 days for SMAP), which is more sensitive to noise, but the robustness of which can be improved through regularization ([25]). The Nyquist variability removes some of the influence of the NDVI climatology prior and thus the DCA NyVOD results are more of a function of the degree of regularization choice (λ). Figures 10a and 10b show the standard deviation of the MTDCA and DCA high frequency values. A pattern emerges which provides insight into how retrievable VOD is under different regularization approaches. The variability of MTDCA NyVOD is higher than that of DCA NyVOD distinctly in tropical and boreal forests. Outside of these forests and in croplands, the NyVOD standard deviation tends to be lower for both algorithms. This implies that the forest biomes need additional constraints on VOD than the brightness temperatures alone can provide (such as an input VOD climatology), even with multi-temporal persistence assumptions.

Estimation of the covariance between SM and VOD high frequency variabilities provides insights into how much compensation may be taking place in inverting for SM and VOD simultaneously. Figure 11 shows a representation of the joint VOD-SM cost function for an example of a dual channel retrieval problem without regularization for a given overpass. In this example, the cost function has an elongated valley. Small amounts of noise will result in variations in retrievals follow the contours of the valley. In the presence of noise, this compensation will result in positive covariance at the Nyquist frequency as shown by the positive VOD-SM relationship at the minimum cost function values (Figure 11).

Given that SM and VOD errors are typically positively correlated (Figure 11 and [25]), we evaluate systematic compensation between VOD and SM by computing the covariance between the SM and VOD at the Nyquist frequency. If the problem is significantly under-determined, this may manifest itself as random variability (and thus as positive covariance) in the signal at high frequencies.

Figure 12 shows the resulting covariance between VOD and SM at the Nyquist frequencies for each product. The covariance rather than the correlation is used to normalize out differences between the DCA's and MTDCA's SM-VOD coupling that are due to the standard deviations of soil moisture and VOD. For the multi-temporal regularization (MTDCA) this covariance is positive on average (mean cov = $1.75 \cdot 10^{-4}$; Figure 12a,c). This trend occurs in forest vegetation classes (Figure S3). Importantly, these results indicate that the multi-temporal algorithm using two satellite overpasses may still be contaminated by errors. However, note that there are cases where positive covariance between soil moisture and VOD on sub-weekly timescales are expected based on predawn soil-plant equilibrium under plant hydraulic theory ([12]). Such may be the case in boreal forests, where the high covariance values for this vegetation class (Figure S3) should not be related to VOD-SM compensation due to errors, as suggested by the high SNR in boreal woodlands (SNR>2; Figures 5 and S3). It should be noted that forested regions with low SNR do show typically positive covariance which may indicate mainly effects of noise. In non-forest regions, where SNR is higher, the MTDCA shows low SM-VOD covariance at the Nyquist frequency. This is consistent with lack of SM-VOD compensating errors when retrievability is high. Also, negative covariance could be expected in semi-arid regions, where negative SM-VOD correlation at short timescales occurs during dry-downs ([13]). This is likely not observed here to as large of a degree as in previous work because we are analyzing the entire time-series, not only dry-downs (Figures S3 and 12).

For the Tikhonov regularization (DCA product) the NySM-NyVOD covariance is slightly negative (mean cov = $-1 \cdot 10^{-4}$; Figure 12b,c). This happens independently of the SNR values (Figures 5, 12 and S3). The trend is consistent through most vegetation classes, except for temperate (cov~0) and boreal forests (cov>0; Figure S3). The exact mechanism leading to the negative covariance is unclear. Potentially, this may result from the Tikhonov regularization having too high of a degree of regularization. This is likely given that the Tikhonov approach in the DCA uses MODIS greenness climatology as a prior. As such, the DCA constrains the ability to assess high frequency VOD variability. Tests indicate that the DCA closely relates to the prior input of NDVI climatology in many places supporting that too much regularization may have been applied in the DCA VOD retrievals (Figure S4).

Despite differences in the algorithms and coupling with soil moisture, the high frequency variability of VOD from both products tends to be positively correlated (except in tropical forests; Figure 13). This indicates that the aforementioned differences may be playing a larger role on the amplitude of variations across frequencies of the variations. Ultimately, the detection of increases and decreases in VOD generally tend to be similar and in phase.

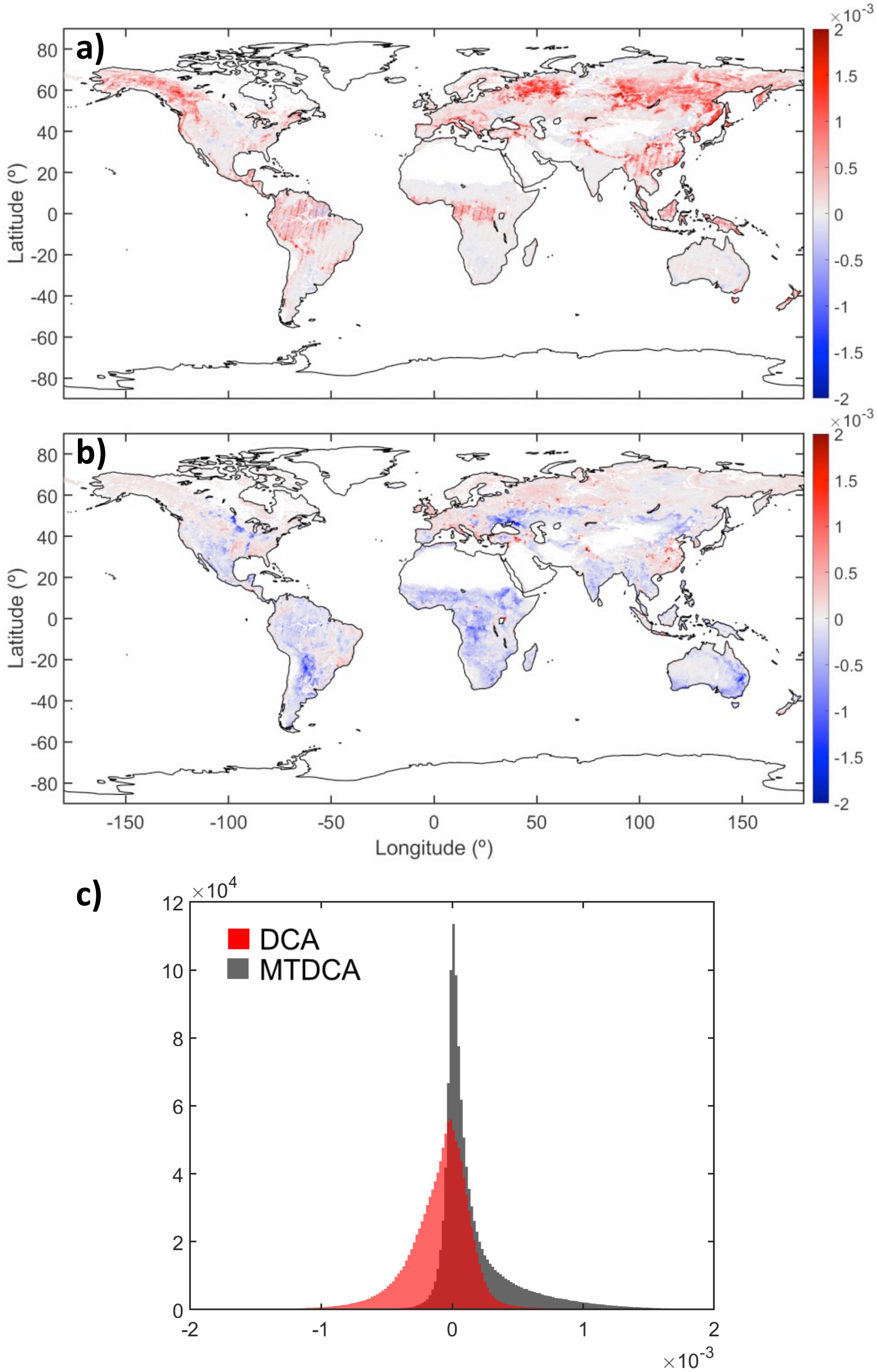

Figure 12. (a) Map of covariance between Nyiquist SM and Nyquist VOD for MTDCA; (b) map of covariance between Nyquist SM and Nyquist VOD for DCA; and (c) histogram comparing the distribution of covariances between Nyquist SM and Nyquist VOD for DCA (red) and MTDCA (grey).

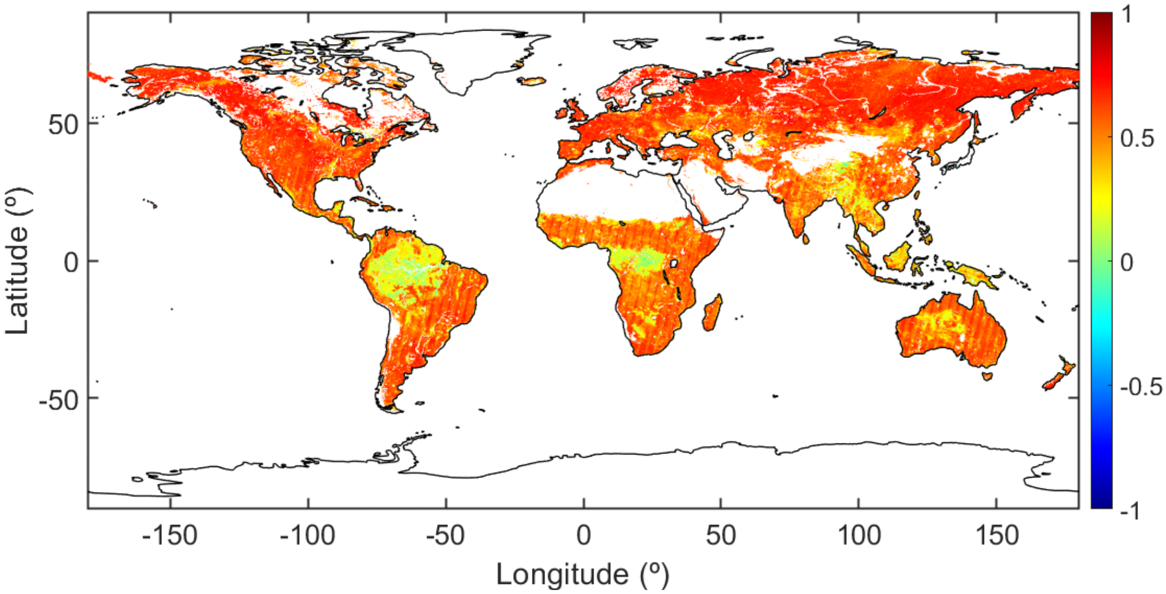

Figure 13. Map of Pearson's correlation coefficient (r) between Nyquist VOD for MTDCA and Nyquist VOD for DCA.

V. CONCLUSIONS

This study evaluates the robustness of VOD retrievals based on SMAP horizontal and vertical polarization brightness temperature measurements in the context of instrument noise. The study also assesses how two different SMAP VOD regularization techniques impact this robustness. Towards these goals, first, a Signal-to-Noise Ratio (SNR) metric is proposed to capture variability above instrument noise; it is used as a complementary metric to the DoI which measures statistical independence of measurements. Second, VOD retrievals and noise from two different VOD regularization approaches using SMAP observations are qualitatively compared across different time scales (annual mean, seasonal amplitude, and high frequency variability). Namely, the SMAP MTDCA and DCA products are compared based on multitemporal and Tikhonov regularization techniques, respectively.

We show that VOD can be robustly retrieved with regularization in regions with lower vegetation density, and with more uncertainty in regions with greater vegetation density. Regions with the highest DoI values correspond to high vegetation densities (i.e., tropical forests; VWC>9 kg/m2), but these values are inflated due to random noise. Moreover, SNR is low based on high TB_v-TB_h correlations, which indicates that the VOD signal in tropical forests is highly impacted by noise due to TB depolarization. Therefore, interpreting DoI alone is misleading in dense vegetation areas: values of DoI~2 are due to random noise, which gives the false impression of having two independent TB sources. We conclude that DoI must be interpreted along with SNR for a holistic understanding of VOD retrievability. In contrast, low-density vegetation areas show high SNR values, with DoI being close to 1.5. The latter indicates need for regularization in order to achieve robust retrievals with enough independent information. Ultimately, our Figure 6 is a guide for where regularized joint retrievals of SM and VOD would produce the smallest errors.

The comparison of multitemporal (MTDCA) and Tikhonov (DCA) regularization techniques shows that their magnitudes of high frequency variability are similar, except for in tropical forests where the variability of MTDCA NyVOD is higher than that of DCA NyVOD. Furthermore, both regularization techniques show generally similar spatial patterns of high frequency coupling of SM-VOD, where covariance tends to be neutral or negative in regions with herbaceous vegetation. This is because regularization reduces noise-based positive correlations between NySM and NyVOD. However, the DCA NySM-NyVOD covariance tends to be lower and more negative on average than that of the MTDCA, even in tropical forests. Based on the more negative NySM-NyVOD coupling and reduced VOD high frequency variability with the DCA product, we suggest that this may be due to too high of a degree of regularization imposed in the DCA Tikhonov algorithm which forces the VOD retrieval to be like the VOD a priori time series based on NDVI climatology. We provide evidence for this by showing that in many global regions, the DCA VOD retrieval is still temporally similar to its VOD a priori constraint. This may over-constrain VOD variability in some cases. Conversely, the MTDCA may require an a priori VOD time series in tropical forests because regularization alone is insufficient to prevent high positive correlations between SM and VOD and high standard deviation of VOD likely due to noise. This indicates that potentially a VOD a priori constraint via the Tikhonov regularization may only be needed in more densely vegetated regions. A more naïve approach like the MTDCA or Sobolev-Norm regularization that does not require an a priori VOD time series may be sufficient for regions with low density vegetation.

Ultimately, the high frequency signals of the DCA and MTDCA VOD time series positively correlate (except for tropical forests). Therefore, despite the differences in VOD retrieval approaches and potential for under and over-regularization in each product, the increases and decreases in

VOD at sub-weekly timescales are in phase between the algorithms. This indicates that the amplitude of variability across different frequencies may be more impacted than the sub-weekly detection of increases and decreases in VOD. More confidence may therefore be exhibited in the use of VOD to detect plant rehydration and water loss rather than the magnitude of these changes. These patterns emerge independent of the regularization approach.

Altogether, from the results presented here, we first recommend the simultaneous application of SNR and DoI metrics for the evaluation of VOD robustness. Second, we suggest further assessing whether the degree of regularization within the SMAP DCA's Tikhonov approach is too high. If so, it can be reduced to capture VOD dynamics where adequate polarization information exists based on TBs, DoI and SNR. This reduction could be addressed by using a spatially varying λ (instead of a global constant value) according to a map of VOD noise (see Figure 2a in [21]). Third, we recommend potentially increasing the regularization in multitemporal retrievals or imposing a priori climatology for noise-dominated regions (mainly tropical forests). We expect that the implementation of these changes can lead to more accurately retrieving SM-VOD dynamics.

Acknowledgment

This work was supported by "la Caixa" Foundation (ID 100010434), under agreement LCF/PR/MIT19/51840001, and by MIT (MIT-Spain Seed Fund). Also, D. Chaparro received financial support from the Ramon Areces foundation postdoctoral grant for life sciences, from the Spanish Ministry of Science, Innovation and Universities and from the European Regional Development Fund (ERDF, EU) through projects PID2020-114623RB-C32, funded by MCIN/ AEI/10.13039/501100011033, MDM-2016-0600, and the "José Castillejo Fellowship" (CAS19/00264). Andrew F. Feldman was supported by an appointment to the NASA Postdoctoral Program at the NASA Goddard Space Flight Center, administered by Universities Space Research Association under contract with NASA. Dara Entekhabi thanks NASA, which provided support in the form of a sponsored research grant (Subcontract No. 1510842).

References

[1] D. Entekhabi *et al.*, "The Soil Moisture Active Passive (SMAP) Mission," *Proceedings of the IEEE*, vol. 98, no. 5, pp. 704–716, May 2010, doi: 10.1109/JPROC.2010.2043918.

[2] Y. H. Kerr *et al.*, "The SMOS Mission: New Tool for Monitoring Key Elements ofthe Global Water Cycle," *Proceedings of the IEEE*, vol. 98, no. 5, pp. 666–687, May 2010, doi: 10.1109/JPROC.2010.2043032.

[3] T. J. Schmugge and T. J. Jackson, "A dielectric model of the vegetation effects on the microwave emission from soils," *IEEE Trans. Geosci. Remote Sensing*, vol. 30, no. 4, pp. 757–760, Jul. 1992, doi: 10.1109/36.158870.

[4] M. Momen *et al.*, "Interacting Effects of Leaf Water Potential and Biomass on Vegetation Optical Depth," *J. Geophys. Res. Biogeosci.*, vol. 122, no. 11, pp. 3031–3046, Nov. 2017, doi: 10.1002/2017JG004145.

[5] N. M. Holtzman *et al.*, "L-band vegetation optical depth as an indicator of plant water potential in a temperate deciduous forest stand," *Biogeosciences*, vol. 18, no. 2, pp. 739–753, Feb. 2021, doi: 10.5194/bg-18-739-2021.

[6] M. Brandt *et al.*, "Satellite passive microwaves reveal recent climate-induced carbon losses in African drylands," *Nat Ecol Evol*, vol. 2, no. 5, Art. no. 5, May 2018, doi: 10.1038/s41559-018-0530-6.

[7] L. Fan *et al.*, "Satellite-observed pantropical carbon dynamics," *Nat. Plants*, vol. 5, no. 9, Art. no. 9, Sep. 2019, doi: 10.1038/s41477-019-0478-9.

[8] A. Mialon *et al.*, "Evaluation of the Sensitivity of SMOS L-VOD to Forest Above-Ground Biomass at Global Scale," *Remote Sensing*, vol. 12, no. 9, Art. no. 9, Jan. 2020, doi: 10.3390/rs12091450.

[9] D. Chaparro, M. Piles, M. Vall-llossera, A. Camps, A. G. Konings, and D. Entekhabi, "L-band vegetation optical depth seasonal metrics for crop yield assessment," *Remote Sensing of Environment*, vol. 212, pp. 249–259, Jun. 2018, doi: 10.1016/j.rse.2018.04.049.

[10] A. Mateo-Sanchis, M. Piles, J. Muñoz, J. Adsuara, A. Pérez-Suay, and G. Camps-Valls, "Synergistic integration of optical and microwave satellite data for crop yield estimation," *Remote Sensing of Environment*, Oct. 2019, doi: 10.1016/j.rse.2019.111460.

[11] S. Sadri, E. F. Wood, and M. Pan, "Developing a drought-monitoring index for the contiguous US using SMAP," *Hydrology and Earth System Sciences*, vol. 22, no. 12, pp. 6611–6626, Dec. 2018, doi: 10.5194/hess-22-6611-2018.

[12] A. F. Feldman, D. J. Short Gianotti, A. G. Konings, P. Gentine, and D. Entekhabi, "Patterns of plant rehydration and growth following pulses of soil moisture availability," Biogeophysics: Ecohydrology, preprint, Oct. 2020. doi: 10.5194/bg-2020-380.

[13] A. F. Feldman *et al.*, "Moisture pulse-reserve in the soil-plant continuum observed across biomes," *Nature Plants*, vol. 4, no. 12, pp. 1026–1033, Dec. 2018, doi: 10.1038/s41477-018-0304-9.

[14] D. S. Lyons, S. Z. Dobrowski, Z. A. Holden, M. P. Maneta, and A. Sala, "Soil moisture variation drives canopy water content dynamics across the western U.S.," *Remote Sensing of Environment*, vol. 253, p. 112233, Feb. 2021, doi: 10.1016/j.rse.2020.112233.

[15] K. Togliatti *et al.*, "Quantitative Assessment of Satellite L-Band Vegetation Optical Depth in the U.S. Corn Belt," *IEEE Geoscience and Remote Sensing Letters*, vol. 19, pp. 1–5, 2022, doi: 10.1109/LGRS.2020.3034174.

[16] K. Togliatti *et al.*, "Satellite L–band vegetation optical depth is directly proportional to crop water in the US Corn Belt," *Remote Sensing of Environment*, vol. 233, p. 111378, Nov. 2019, doi: 10.1016/j.rse.2019.111378.

[17] Y. Zhang, S. Zhou, P. Gentine, and X. Xiao, "Can vegetation optical depth reflect changes in leaf water potential during soil moisture dry-down events?," *Remote Sensing of Environment*, vol. 234, p. 111451, Dec. 2019, doi: 10.1016/j.rse.2019.111451.

[18] A. G. Konings, K. A. McColl, M. Piles, and D. Entekhabi, "How Many Parameters Can Be Maximally Estimated

From a Set of Measurements?," *IEEE Geosci. Remote Sensing Lett.*, vol. 12, no. 5, pp. 1081–1085, May 2015, doi: 10.1109/LGRS.2014.2381641.

[19] T. Mo, B. J. Choudhury, T. J. Schmugge, J. R. Wang, and T. J. Jackson, "A model for microwave emission from vegetation-covered fields," *Journal of Geophysical Research: Oceans*, vol. 87, no. C13, pp. 11229–11237, 1982, doi: 10.1029/JC087iC13p11229.

[20] R. Bindlish, T. Jackson, M. Cosh, T. Zhao, and P. O'Neill, "Global Soil Moisture From the Aquarius/SAC-D Satellite: Description and Initial Assessment," *IEEE Geoscience and Remote Sensing Letters*, vol. 12, no. 5, pp. 923–927, May 2015, doi: 10.1109/LGRS.2014.2364151.

[21] J. Chaubell *et al.*, "Regularized Dual-Channel Algorithm for the Retrieval of Soil Moisture and Vegetation Optical Depth From SMAP Measurements," *IEEE Journal of Selected Topics in Applied Earth Observations and Remote Sensing*, vol. 15, pp. 102–114, 2022, doi: 10.1109/JSTARS.2021.3123932.

[22] B. Li and S. P. Good, "Information-based uncertainty decomposition in dual-channel microwave remote sensing of soil moisture," *Hydrol. Earth Syst. Sci.*, vol. 25, no. 9, pp. 5029–5045, Sep. 2021, doi: 10.5194/hess-25-5029-2021.

[23] A. Ebtehaj and R. L. Bras, "A physically constrained inversion for high-resolution passive microwave retrieval of soil moisture and vegetation water content in L-band," *Remote Sensing of Environment*, vol. 233, p. 111346, Nov. 2019, doi: 10.1016/j.rse.2019.111346.

[24] S. Zwieback, D. D. Bosch, M. H. Cosh, P. J. Starks, and A. Berg, "Vegetation–soil moisture coupling metrics from dual-polarization microwave radiometry using regularization," *Remote Sensing of Environment*, vol. 231, p. 111257, Sep. 2019, doi: 10.1016/j.rse.2019.111257.

[25] A. Feldman, D. Chaparro, and D. Entekhabi, "Error Propagation in Microwave Soil Moisture and Vegetation Optical Depth Retrievals," *IEEE J. Sel. Top. Appl. Earth Observations Remote Sensing*, vol. 14, pp. 11311–11323, 2021, doi: 10.1109/JSTARS.2021.3124857.

[26] L. Gao, A. Ebtehaj, M. J. Chaubell, M. Sadeghi, X. Li, and J.-P. Wigneron, "Reappraisal of SMAP inversion algorithms for soil moisture and vegetation optical depth," *Remote Sensing of Environment*, vol. 264, p. 112627, Oct. 2021, doi: 10.1016/j.rse.2021.112627.

[27] A. G. Konings, M. Piles, K. Rötzer, K. A. McColl, S. K. Chan, and D. Entekhabi, "Vegetation optical depth and scattering albedo retrieval using time series of dual-polarized L-band radiometer observations," *Remote Sensing of Environment*, vol. 172, pp. 178–189, Jan. 2016, doi: 10.1016/j.rse.2015.11.009.

[28] R. Fernandez-Moran *et al.*, "SMOS-IC: An Alternative SMOS Soil Moisture and Vegetation Optical Depth Product," *Remote Sensing*, vol. 9, no. 5, Art. no. 5, May 2017, doi: 10.3390/rs9050457.

[29] J.-P. Wigneron, P. Waldteufel, A. Chanzy, J.-C. Calvet, and Y. Kerr, "Two-Dimensional Microwave Interferometer Retrieval Capabilities over Land Surfaces (SMOS Mission)," *Remote Sensing of Environment*, vol. 73, no. 3, pp. 270–282, Sep. 2000, doi: 10.1016/S0034-4257(00)00103-6.

[30] A. G. Konings, M. Piles, N. Das, and D. Entekhabi, "L-band vegetation optical depth and effective scattering albedo estimation from SMAP," *Remote Sensing of Environment*, vol. 198, pp. 460–470, Sep. 2017, doi: 10.1016/j.rse.2017.06.037.

[31] A. F. Feldman and D. Entekhabi, "Smap Vegetation Optical Depth Retrievals Using The Multi-Temporal Dual-Channel Algorithm," in *IGARSS 2019 - 2019 IEEE International Geoscience and Remote Sensing Symposium*, Yokohama, Japan, Jul. 2019, pp. 5437–5440. doi: 10.1109/IGARSS.2019.8899014.

[32] A. Al Bitar *et al.*, "The global SMOS Level 3 daily soil moisture and brightness temperature maps," *Earth System Science Data*, vol. 9, no. 1, pp. 293–315, Jun. 2017, doi: 10.5194/essd-9-293-2017.

[33] L. Gao, M. Sadeghi, and A. Ebtehaj, "Microwave retrievals of soil moisture and vegetation optical depth with improved resolution using a combined constrained inversion algorithm: Application for SMAP satellite," *Remote Sensing of Environment*, vol. 239, p. 111662, Mar. 2020, doi: 10.1016/j.rse.2020.111662.

[34] ONeill, Peggy E. *et al.*, "SMAP Enhanced L2 Radiometer Half-Orbit 9 km EASE-Grid Soil Moisture, Version 5." NASA National Snow and Ice Data Center DAAC, 2021. doi: 10.5067/LOT311EZHH8S.

[35] A. N. Tikhonov, "On the solution of ill-posed problems and the method of regularization," p. 5.

[36] Huffman, G.J., E.F. Stocker, D.T. Bolvin, E.J. Nelkin, & Jackson, T. (2019), GPM IMERG Final Precipitation L3 1 day 0.1 degree x 0.1 degree V06, Edited by Andrey Savtchenko, Greenbelt, MD, Goddard Earth Sciences Data and Information Services Center (GES DISC), Accessed: 1st December 2021. Doi: 10.5067/GPM/IMERGDF/DAY/06.

[37] J. Dong, W. T. Crow, and R. Bindlish, "The Error Structure of the SMAP Single and Dual Channel Soil Moisture Retrievals," *Geophys. Res. Lett.*, vol. 45, no. 2, pp. 758–765, Jan. 2018, doi: 10.1002/2017GL075656.

[38] Chaubell, M. Julian, Chan, Steven, Dunbar, R. Scott, Peng, Jinzheng, and Yueh, Simon, "SMAP Enhanced L1C Radiometer Half-Orbit 9 km EASE-Grid Brightness Temperatures, Version 2." NASA National Snow and Ice Data Center DAAC, 2018. doi: 10.5067/0DGGEWUC6MLY.

[39] ONeill, Peggy E., Chan, Steven, Njoku, Eni G., Jackson, Tom, Bindlish, Rajat, and Chaubell, M. Julian, "SMAP Enhanced L3 Radiometer Global Daily 9 km EASE-Grid Soil Moisture, Version 4." NASA National Snow and Ice Data Center DAAC, 2020. doi: 10.5067/NJ34TQ2LFE90.

[40] S. Chan and R. S. Dunbar, "Enhanced Level 1C Radiometer Data Product Specification Document," p. 55.

[41] A. Feldman, A. Konings, M. Piles, and D. Entekhabi, "The Multi-Temporal Dual Channel Algorithm (MT-DCA)." Zenodo, Oct. 19, 2021. doi: 10.5281/zenodo.5619583.

[42] Y. H. Kerr, P. Waldteufel, P. Richaume, I. Davenport, P. Ferrazzoli, and J. P. Wigneron, "SMOS level 2 processor soil moisture algorithm theoretical basis document (ATBD)," *CBSA, UoR, TV and INRA, Toulouse, Tech. Rep. SO-TN-ARR-L2PP-0037*, vol. 3, 2006.

[43] M. J. Baur, T. Jagdhuber, A. F. Feldman, D. Chaparro, M. Piles, and D. Entekhabi, "Time-variations of zeroth-order vegetation absorption and scattering at L-band," *Remote Sensing of Environment*, vol. 267, p. 112726, Dec. 2021, doi: 10.1016/j.rse.2021.112726.
[44] S. Watanabe, "Information Theoretical Analysis of Multivariate Correlation," *IBM Journal of Research and Development*, vol. 4, no. 1, pp. 66–82, Jan. 1960, doi: 10.1147/rd.41.0066.
[45] D. Chaparro *et al.*, "Sensitivity of L-band vegetation optical depth to carbon stocks in tropical forests: a comparison to higher frequencies and optical indices," *Remote Sensing of Environment*, vol. 232, p. 111303, Oct. 2019, doi: 10.1016/j.rse.2019.111303.

David Chaparro received the Graduate degree in biology from the Universitat Autònoma de Barcelona, Barcelona, Spain, in 2011, the dual M.S. degrees in remote sensing and geographic information systems and in terrestrial ecology from the Center for Ecological Research and Forestry Applications, Barcelona, Spain, in 2012 and 2013, respectively, and the Ph.D. degree in telecommunication engineering from the Universitat Politècnica de Catalunya, Barcelona, Spain, in 2018. He is currently postdoctoral researcher with the Microwaves and Radar Institute at the German Aerospace Center (DLR). He is working on vegetation moisture retrievals from satellites and exploring new frameworks to study the soil-plant-atmosphere continuum from satellite sensor sinergies. His research interests include earth observation from microwave radiometers and optical sensors to develop environmental research and applications.

Andrew F. Feldman (Student Member, IEEE) received the B.S. and M.S. degrees in civil engineering from Drexel University, Philadelphia, PA, USA, in 2016, and the S.M. and Ph.D. degrees in civil and environmental engineering from the Massachusetts Institute of Technology (MIT), Cambridge, MA, USA, in 2018 and 2021, respectively. He is currently a NASA Postdoctoral Program Fellow with NASA Goddard Space Flight Center, Biospheric Sciences Laboratory, Greenbelt, MD, USA. His research interests include land-surface hydrology, terrestrial ecosystem science, and microwave remote sensing.

Julian Chaubell received the Bachelor of Science degree in mathematics from the University of Mar del Plata, Buenos Aires, Argentina, in 1997, and the Ph.D. degree in applied and computational mathematics from the California Institute of Technology, Pasadena, CA, USA, in 2004. He is currently with the Jet Propulsion Laboratory, California Institute of Technology, Pasadena, CA. His research interests include the forward modelling of radar and radiometer measurements as well as retrieval of the geophysical quantity from those measurements.

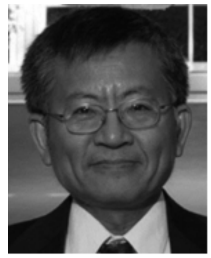

Simon H. Yueh received the Ph.D. degree in electrical engineering from the Massachusetts Institute of Technology, Cambridge, MA, USA, in January 1991. He is currently a Senior Research Scientist and SMAP Project Scientist with the Jet Propulsion Laboratory, California Institute of Technology, Pasadena, CA, USA. Dr. Yueh is the Editor-in-Chief for the IEEE TRANSACTIONS ON GEOSCIENCE AND REMOTE SENSING.

Dara Entekhabi (Fellow, IEEE) received the B.S. and dual M.S. degrees in geography from Clark University, Worcester, MA, USA, in 1983, 1985, and 1988, respectively, and the Ph.D. degree in civil and environmental engineering from the Massachusetts Institute of Technology (MIT), Cambridge, MA, USA, in 1990. He is currently a Professor with the Department of Civil and Environmental Engineering and the Department of Earth, Atmospheric and Planetary Sciences, MIT. He is the Science Team lead for the National Aeronautics and Space Administration's Soil Moisture Active and Passive mission that was launched January 31, 2015. His research interests include terrestrial remote sensing, data assimilation, and coupled land–atmosphere systems modeling. Prof. Entekhabi is a Fellow of the American Meteorological Society and the American Geophysical Union. He is a member of the National Academy of Engineering.